energies

MDPI

Article

Research on the Carrier Characteristics of Power Cables Considering the Aging Status of Insulation and Semiconducting Layers

Xiaohua Yang [1], Zixuan Wang [2], Jiahao Li [1], Ming Wu [2,*], Guanpan Wang [1], Xueting Gao [2] and Jinghui Gao [2,*]

[1] Measurement Center of Yunnan Power Grid Co., Ltd., Kunming 650051, China
[2] National Key Laboratory of Electrical Materials and Insulation, Xi'an Jiaotong University, Xi'an 710049, China
* Correspondence: wuming@xjtu.edu.cn (M.W.); gaojinghui@xjtu.edu.cn (J.G.)

Abstract: The 10 kV XPLE cable is widely used in highly cabled transmission and distribution networks. It is necessary to closely monitor the transient current, harmonic content, and electric field distribution of each layer of the insulation and semiconductive layers of the cable when they age and deteriorate, so as to promptly carry out circuit breaking treatment and prevent safety accidents. Considering the frequency sensitivity and dielectric sensitivity of the distributed R_{unit}, L_{unit}, G_{unit}, and C_{unit} parameters of long cables, this paper quantitatively analyzes the frequency variation of 10 kV cable parameters under different aging states. Reconstructing the frequency variation process of typical electrical quantities through MATLAB PSCAD joint simulation, constructing fault circuits for cable insulation and semiconducting layers, obtaining transient currents in each layer of the cable under aging conditions, and conducting total harmonic distortion (THD) analysis to provide theoretical guidance for the subsequent monitoring and fault diagnosis of distribution cable status.

Keywords: aging; cable; distributed parameters; impedance spectrum; PSCAD/EMTDC

check for updates

Citation: Yang, X.; Wang, Z.; Li, J.; Wu, M.; Wang, G.; Gao, X.; Gao, J. Research on the Carrier Characteristics of Power Cables Considering the Aging Status of Insulation and Semiconducting Layers. *Energies* **2024**, *17*, 5655. https://doi.org/10.3390/en17225655

Academic Editor: José Matas

Received: 21 October 2024
Revised: 4 November 2024
Accepted: 7 November 2024
Published: 12 November 2024

Copyright: © 2024 by the authors. Licensee MDPI, Basel, Switzerland. This article is an open access article distributed under the terms and conditions of the Creative Commons Attribution (CC BY) license (https://creativecommons.org/licenses/by/4.0/).

1. Introduction

In recent years, the rate of underground cabling in China's urban power transmission and distribution networks has been steadily increasing. However, this has also led to a rise in the failure rate of the cable's insulation layer [1] and semiconductive layer [2]. XLPE cables, during both manufacturing and operation, are inevitably affected by factors such as production and installation processes [3]. Additionally, during operation, the insulation layer is subjected to electrical, thermal, and mechanical stresses, as well as high-frequency overvoltages [4], which can cause defects or structural damage to the XLPE insulation [5]. Such damage severely compromises the cable's insulation performance. Once internal degradation phenomena [6] such as electrical treeing, water treeing, or charge accumulation occur, they can lead to irreversible cable failures under lightning overvoltages or switching overvoltage [7] impulses caused by high-frequency switching operations.

Due to the high cost of simulating fault processes in real cable operations and the difficulty in eliminating non-subjective factors such as soil conditions, using simulation to model cable faults has become one of the most effective methods. After obtaining circuit simulation data, software such as MATLAB and COMSOL Multiphysics V6.1 can be combined to locate fault points [8,9]. Additionally, wavelet transform and neural networks can be employed for fault pattern recognition [10].

In power transmission and distribution networks with a high degree of cable installation, improving cable quality and reducing fault rates are particularly important. During the aging process of polymer materials, changes in dielectric parameters [11] lead to simultaneous variations in the distributed parameters R_{unit}, L_{unit}, G_{unit}, and C_{unit} [12], which directly affect the transmission characteristics of power line channels [13–15]. As a result, cable aging can impact the channel transfer function to some extent, making it possible to

detect and analyze changes in these functions to infer whether anomalies exist in the power line's condition. This paper establishes a transmission line model to study aging-related faults in 10 kV single-core power cables. Through comparative analysis of the current transmission characteristics between faulty and non-faulty circuits in PSCAD, this study identifies key parameters typical of single-core power cable faults, providing valuable references for practical measurement and research.

The important physical quantities involved in this article are shown in Table 1.

Table 1. Important physical quantities.

Parameters	Symbols	Units
Unit length resistance	R_{unit}	Ω/m
Unit length inductance	L_{unit}	H/m
Unit length capacitance	C_{unit}	F/m
Characteristic impedance	Z_C	Ω
Propagation constant	γ	1
Relative permittivity	ε	1
Dielectric loss tangent	tanδ	1
Penetration depth	ξ	mm
Wave velocity	v	m/s
Rise time	t_r	μs

2. Impact of XLPE Aging on Cable Distributed Parameters

2.1. Changes in Dielectric Properties During Aging

Setting the thermal aging temperature of the material to 125 °C, the average core temperature of a 35 kV cable under normal operating conditions is approximately 50–75 °C. Assuming 65 °C as the actual temperature of the cable's insulation layer, a rough estimation can be made that accelerated thermal aging for 120 days at 125 °C is equivalent to around 20 years of normal operation at 65 °C.

The dielectric properties were tested using the Concept 80 broadband dielectric spectroscopy system, with the frequency range set between 1 kHz and 10 MHz, and the testing temperature set at room temperature. The operating principle of the broadband dielectric spectroscopy system is illustrated in Figure 1a. Samples were selected in four different aging states: unaged and after 30, 60, and 90 days of accelerated aging, with results shown in Figure 1b.

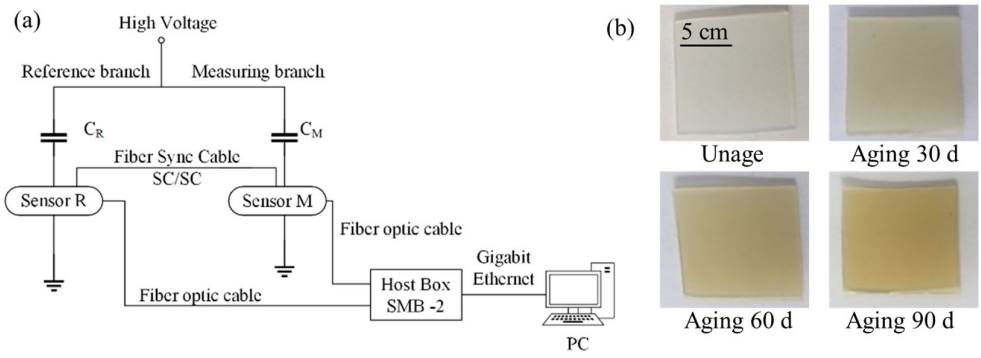


Figure 1. (**a**) The Concept 80 broadband dielectric spectroscopy test system measurement principle. (**b**) The color change of XLPE after thermal aging.

During prolonged thermal aging, polyethylene materials experience not only changes in mechanical properties but also degradation in dielectric performance. This includes an increase in dielectric constant and dielectric losses, which can affect the stability and reliability of the cable systems. By studying the relationship between the dielectric constant, dielectric loss, and aging time of XLPE, the thermal aging resistance of XLPE is analyzed from an electrical performance perspective.

Figure 2 shows that both the dielectric constant and loss factor of XLPE materials increase with aging time. A significant upward trend in the loss factor is observed around 60 days of aging, with a two-order-of-magnitude increase by 120 days of aging. This behavior can be attributed to the thermal aging reaction products, which contain a large number of carbonyl and hydroxyl groups. These groups introduce polar functional groups at the ends of the molecular chains, leading to relaxation polarization under the influence of an electric field. The presence of these polar functional groups results in energy dissipation as the electric field overcomes internal viscous resistance, thereby increasing dielectric losses [16]. Additionally, the carbonyl and hydroxyl polar functional groups can readily undergo intrinsic dissociation, generating conductive ions that increase the concentration of charge carriers, further elevating the material's conductivity and associated conductive losses.

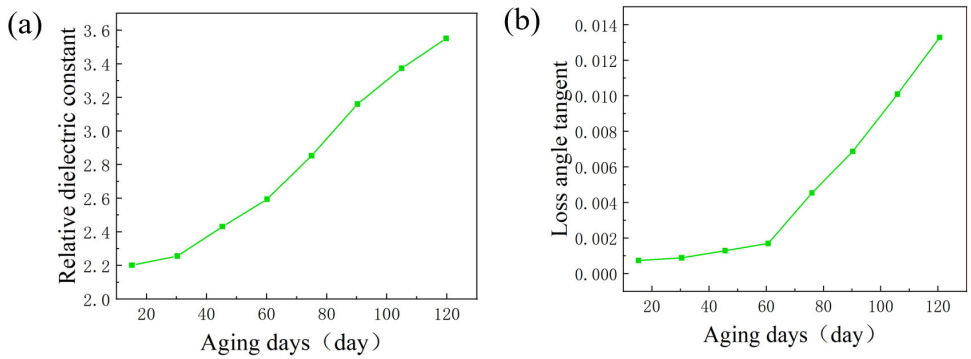


Figure 2. The relationship between dielectric parameters of XLPE and aging time. (**a**) Relative dielective constant. (**b**) Diele.

At this stage, the factors that cause a sudden change in the degradation rate of the material are as follows:

1. When free radicals accumulate to a certain extent, a self-catalytic process of chain oxidation reaction will be formed, causing the material to enter a rapid degradation state. 2. The cross-linked structure of XLPE is destroyed at high temperatures. Upon reaching a certain temperature or aging time, the rate of cross-linking bond breakage accelerates, leading to the degradation of molecular chains and a significant increase in dielectric loss. 3. During the thermal aging process, micropores gradually form, absorbing moisture or impurities from the surrounding environment, further leading to a decrease in electrical performance. 4. The polymer inside XLPE degrades to form carbide products. When the degradation products accumulate to a certain amount and form a through conductive path, the dielectric loss will rapidly increase.

2.2. Effects of Aging on Cable Parameters

High-frequency signals experience attenuation in cables, as illustrated in Figure 3a. On one hand, the resistance of the cable core contributes to signal loss; on the other hand, the capacitance formed between the cable and the ground also results in additional losses. In Figure 3a, Z represents the impedance of the core conductor, which includes both the resistance and inductance of the core. For high-frequency signals, the skin effect becomes significant, making it inadequate to use the standard copper resistivity as the resistance per unit length. This approach can lead to substantial errors; therefore, it is essential to consider the effective cross-sectional area [17] of the current flowing through the core conductor, as illustrated in Figure 3b. Taking a solid copper conductor at 20 °C as an example, investigate the variation in its skin depth between 50 Hz and 10,000 Hz, as shown in the Figure 3c. The skin depth at 50 Hz is 9.3458 mm, while at 10,000 Hz it drops to 0.6608 mm.

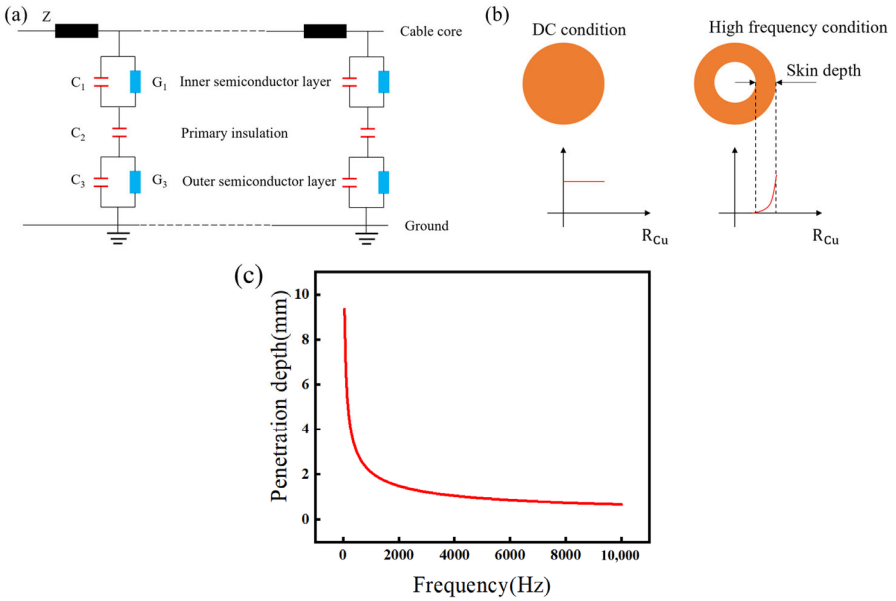


Figure 3. (**a**) High-frequency signal attenuation equivalent model. (**b**) The current distribution of skin effect is considered. (**c**) Penetration depth at different frequencies.

The current and voltage at the beginning and end of the cable satisfy the following relationship:

$$\begin{cases} U_2 = U_1 ch\gamma l - Z_C I_1 sh\gamma l \\ I_2 = -\frac{U_2}{Z_C} sh\gamma l + I_1 ch\gamma l \end{cases} \quad (1)$$

where l represents the length of the cable, Z_C denotes the characteristic impedance of the cable, and γ is the propagation constant of the cable. Therefore, this equation allows for the determination of the voltage and current at every point along the cable during operation. Assuming a load with impedance Z_L is connected at the end of the power line, the input impedance as viewed from the beginning of the cable is given by the following:

$$Z_{in} = Z_C \frac{Z_L + Z_C \tan h(\gamma l)}{Z_C + Z_L \tan h(\gamma l)} \quad (2)$$

Considering the case in which the cable end is open-circuited, the load impedance Z_L approaches infinity. In this scenario, the characteristic impedance of the cable Z_C can be effectively neglected in comparison to the load impedance Z_L. Thus, the input impedance as viewed from the beginning of the cable is given by the following:

$$Z_{inoc} = Z_C \frac{1}{\tan h(\gamma l)} \quad (3)$$

Considering the case in which the cable end is short-circuited, and the load impedance Z_L is zero. In this situation, the input impedance as viewed from the beginning of the cable is given by the following:

$$Z_{insc} = Z_C \cdot \tan h(\gamma l) \quad (4)$$

By simultaneously solving the expressions for Z_{inoc} and Z_{insc}, the characteristic impedance Z_0 and propagation constant γ of the cable can be determined. The propagation constant γ is a complex number, where the real part represents the attenuation constant α of the cable, and the imaginary part represents the phase constant β [18].

$$Z_0 = \sqrt{Z_{inoc} \cdot Z_{insc}} \gamma = \frac{1}{1} \operatorname{arctanh} \sqrt{\frac{Z_{insc}}{Z_{inoc}}} \quad (5)$$

Figure 4 shows the effect of aging of XLPE on characteristic impedance and attenuation. Under different aging conditions, the characteristic impedance decreases with increasing

aging duration. At a frequency of 1 MHz, the characteristic impedance decreases by 22.7% from day 0 to day 120. Conversely, the attenuation constant increases with the aging duration; at frequencies of 100 kHz, 1 MHz, and 10 MHz, the attenuation constant after 120 days of aging increases by 31.87%, 41.38%, and 80%, respectively, compared to the unaged state. Additionally, it can be observed that as the frequency increases, both the attenuation constant and the differences in attenuation constants before and after aging also increase.

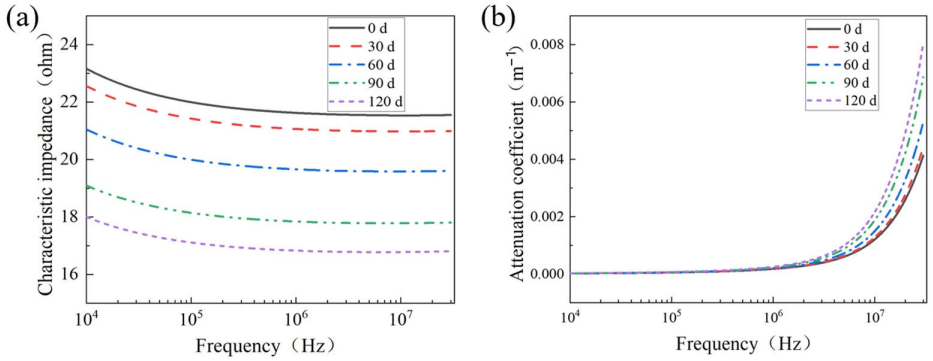


Figure 4. Change of (**a**) characteristic impedance and (**b**) attenuation coefficient of XLPE under different frequencies before and after aging.

Figure 5 shows the effect of aging of XLPE on wave velocity. After 100 kHz, the wave speed remains relatively constant. Specifically, at a frequency of 1 MHz, the wave speed before aging is 1.76×10^8 m/s, while after 120 days of aging, it decreases to 1.45×10^8 m/s, resulting in a change of 21.38%.

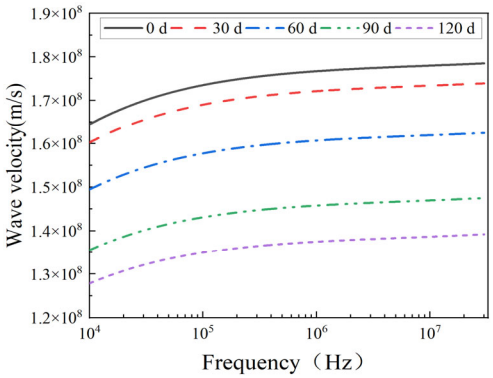


Figure 5. Wave velocity and frequency of XLPE before and after aging.

Among the secondary parameters of the cable, the attenuation constant exhibits the most significant change, increasing by 41.38% at 1 MHz. As the most sensitive parameter, the metal shielding and core wire form a capacitor-like structure, where further increases in capacitance lead to the formation of a capacitive impedance pathway between the core wire and the grounded metal shield. Consequently, the ground impedance decreases with increasing frequency, making this effect more pronounced at high frequencies. The variations in characteristic impedance magnitude and wave speed are approximately between 20% and 22%.

The input impedance spectrum of the 10 kV cable under aging conditions was obtained, with the cable length set to 100 m. Figure 6a,b shows the magnitude and phase spectra of the input impedance at the beginning of the cable before and after aging. The impedance magnitude and phase spectra of the cable exhibit periodic occurrences of significant maxima and minima. Near the maxima of the impedance magnitude spectrum and the zero-crossings of the impedance phase spectrum, the variations in impedance

are particularly rapid. The exponential operator $e^{-2\gamma le}$ is primarily responsible for the rapid changes observed in the impedance spectrum. Additionally, the maxima of both the impedance magnitude and phase spectra show a characteristic decay with increasing frequency. As aging progresses, the wave speed of the cable continuously decreases, and the period of the impedance spectrum extremes is given by $T_Z = v/2l$. Thus, aging also impacts the periodicity of the impedance spectrum.

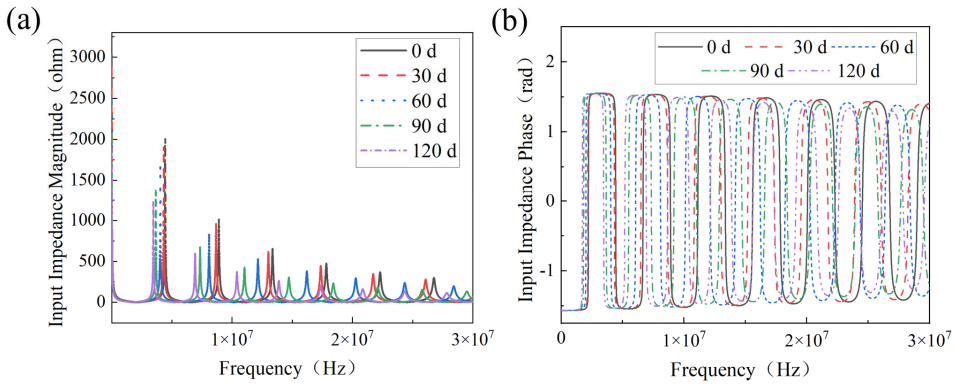


Figure 6. Initial impedance spectrum variation before and after aging. (**a**) Impedance amplitude at the head-end. (**b**) Impedance phase at the head-end.

For the amplitude frequency characteristics, the peak shows a 39.6% attenuation, and the curve shifts toward the low-frequency range by 986 kHz. For the phase frequency characteristics, there was no significant attenuation, but the curve shifted toward the high-frequency band by 496 kHz.

3. Impact of Semiconductive Layer Aging on Cable Distributed Parameters

3.1. Changes in Dielectric Properties During Aging

The change in the dielectric properties of the semiconductive layer during aging are shown in Figure 7. With the increase in aging days, the relative permittivity of the semiconductive layer shows a rising trend. After aging, the changes in the cable shielding layer are more pronounced in the low- and mid-frequency ranges, with variations exceeding three orders of magnitude. In contrast, the changes in the high-frequency range are relatively smaller, approximately an order of magnitude increase.

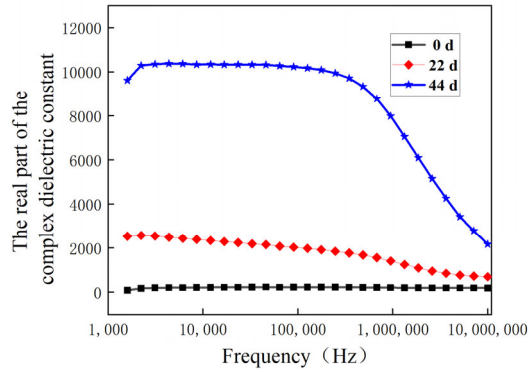


Figure 7. Spectrogram of dielectric constant of a semiconductive shield at room temperature.

With the extension of the aging time, the cross-linking degree of the EVA matrix (materials of the semiconductive layer) increases, which inhibits contact between the carbon black particles. The composite system of carbon black particles and EVA forms a microcapacitive structure [19], resulting in an increase in the dielectric constant of the semiconductive material over time. However, as the test frequency increases, the relaxation

polarization cannot keep pace with the changes in the electric field, leading to a decrease in the dielectric constant of the semiconductive material with rising test frequency.

Figure 8 shows the dielectric properties of EVA under different temperatures and different aging states. In the low-temperature range, the polar molecules in the EVA-based semiconductive shielding layer exhibit weak thermal motion and are in a frozen state, resulting in a long relaxation time. The polar molecular chains are unable to align quickly in response to the applied alternating electric field, leading to dielectric losses. As molecular thermal motion increases, the relaxation time decreases, allowing relaxation polarization related to thermal motion to be established rapidly. Consequently, there is an observable increase in the relative permittivity with the rising temperature of the semiconductive shield.

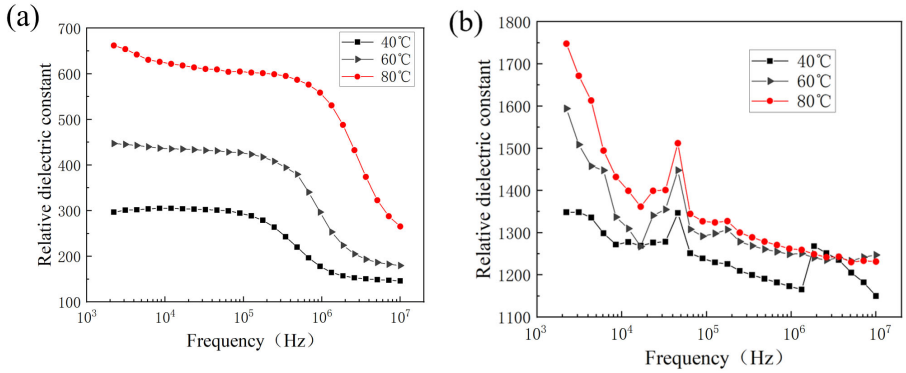


Figure 8. Comparison of relative dielectric constant semiconducting layers at different temperatures. (**a**) Before aging. (**b**) After aging 28 days.

After aging, the EVA-based semiconductive shielding layer still shows this trend, but it is less pronounced compared to the unaged state. The primary reason is that, with the extension of the aging time, the cross-linking degree of the EVA matrix increases, inhibiting contact between carbon black particles. The composite system of carbon black particles and EVA forms a microcapacitive structure, which plays a major role in changes to the dielectric constant. As a result, the contribution of the temperature-induced reduction in relaxation time to the increase in dielectric constant is relatively minor.

1. With the degradation of EVA matrix, carbon black particles may transition from a uniformly dispersed state to an aggregated state, forming larger particle aggregates, ultimately leading to changes in the current path and affecting the overall dielectric performance. 2. Under aging conditions, high temperature and oxidative environment lead to surface oxidation of carbon black particles, causing molecular chain breakage and cross-linking reactions in the EVA matrix, changing its chemical properties and surface structure. The skin effect may be enhanced, causing current to be more concentrated on the surface and resulting in a decrease in the overall dielectric constant [20].

3.2. Effect of Aging on Cable Parameters

During the aging process of the semiconductive shielding layer, the dielectric constant underwent significant changes, which also affected the channel characteristics. By incorporating the dielectric constants measured at 0 days, 22 days, and 44 days into the transmission line model, the characteristic changes in the cable parameters are illustrated in Figure 9.

The characteristic impedance decreases with the increase in aging days. At a frequency of 1 MHz, the characteristic impedance of the semiconductive shielding layer decreases by 3.3% after 44 days of aging. However, after 28 days of aging, the reduction in characteristic impedance is minimal, showing almost no change. As a result, it is challenging to use characteristic impedance as a factor to differentiate the degradation level of the semiconductive shielding layer.

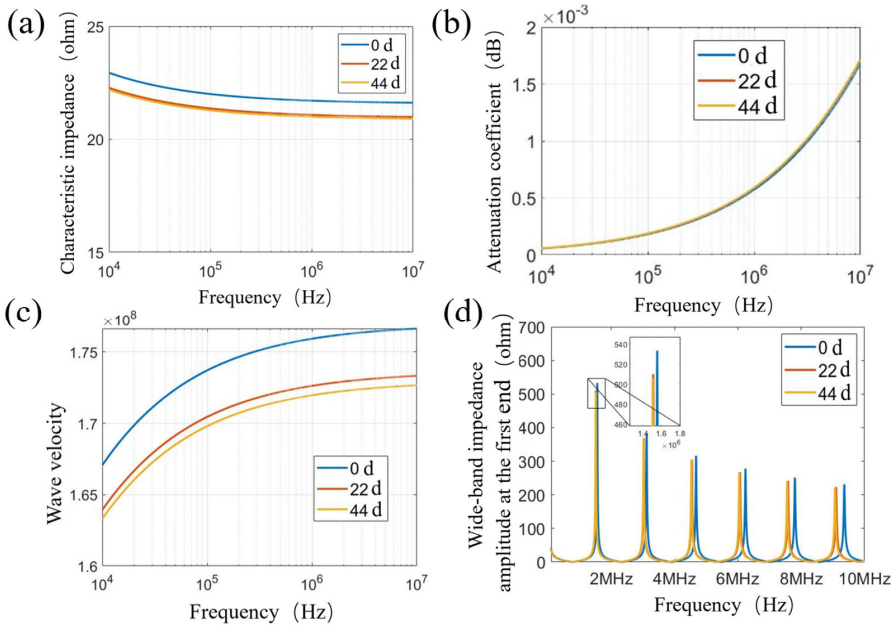


Figure 9. Effect of semiconductive layer aging on the cable parameters. (**a**) Characteristic impedance, (**b**) attenuation, (**c**) wave velocity, (**d**) wide-band impedance amplitude at the first end.

The attenuation constant increases with the number of aging days. At frequencies of 100 kHz, 1 MHz, and 10 MHz, the attenuation constants of the semiconductive shielding layer after 44 days of aging increase by 3.2%, 1.8%, and 2.3%, respectively, compared to the unaged state. Specifically, at 1 MHz, the wave speed before aging is 1.76×10^8 m/s, while after 44 days of aging, it decreases to 1.70×10^8 m/s, reflecting a change of 3.5%. The peak value and peak frequency of the input impedance magnitude at the beginning of the cable also exhibit significant changes, with the peak frequency shifting to the left. After 44 days of aging, the magnitude of the first peak decreases by 7.4% compared to the previous state.

The characteristic impedance, attenuation constant, wave speed, and other parameters exhibit significant changes in the early stages of aging, followed by relatively minor variations. Among these, the increase in the order of the relative permittivity occurs rapidly, leading to corresponding changes in the characteristic impedance and propagation constant. However, once the order of the relative permittivity reaches 10^3, it no longer plays a decisive role in determining these parameters. At this stage, $Z_0 \neq \sqrt{\frac{\mu}{\varepsilon}}$ and $\gamma \neq \sqrt{\frac{1}{\mu\varepsilon}}$.

4. Transient Current Simulation of Cable Layers Under Typical Aging Conditions

4.1. MATLAB-PSCAD Model Development

In this section, a 10 kV distribution cable is selected, and the operating condition is set to accelerated aging for 90 days (severe aging, nearing failure), with the model shown in Figure 10. The frequency-dependent data of the cable parameters after aging are extracted, and a joint simulation using MATLAB ver. 2022a and PSCAD V5 is conducted to investigate the transient current distribution characteristics of the cable under this condition. The cable line operates at a voltage level of 10 kV with a three-phase alternating current, where the voltage rise time is 0.5 s. The alternating current is split into three phases (A, B, and C) through a busbar, forming a three-loop cable system. The metal sheath is configured such that one end is directly grounded while the other end is connected to protective ground. Phase A is designated as the aged phase.

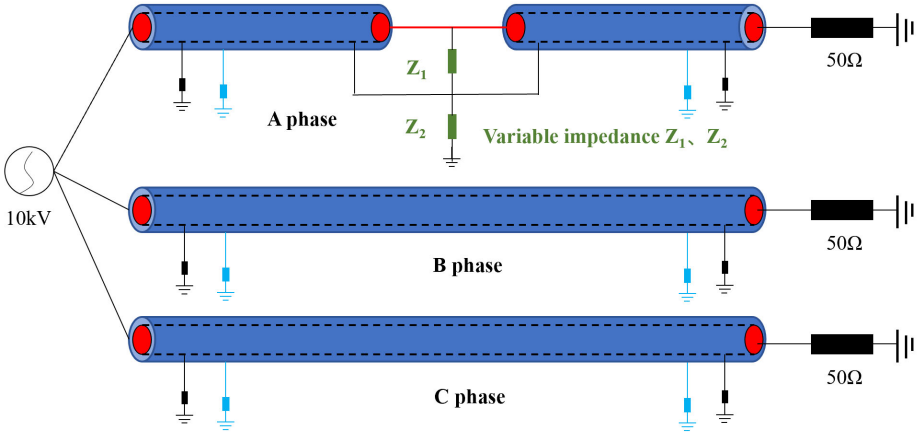


Figure 10. Modeling of aging circuit of 10 kV single-core multiloop cable.

4.2. Results and Discussion

When aging failures occur in the cable, the aged phase experiences failure, resulting in the currents of the conductor layer, shielding layer, and sheath layer as shown in Figure 11. In extreme cases, a loop forms radially along the cable, leading to induced currents between the conductor, shielding, and sheath. The initial current polarity in the sheath layer exhibits a reversal, while the initial polarities of the conductor current and shielding current remain unchanged but are significantly amplified.

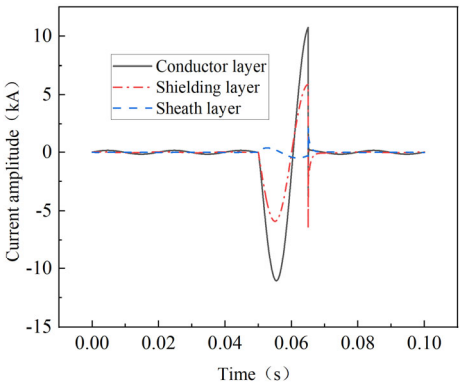


Figure 11. Current distribution at each layer of the fault loop.

The occurrence of aging failures triggers induced pulse signals. Although these signals have a very short duration, the rise time T_r of the pulse and the step-up ΔU exhibit a high sensitivity to the cable length L. By varying the cable lengths to 700 m, 1000 m, 1500 m, and 3000 m and comparing the results with those of a 500 m long cable, the findings are illustrated in Figure 12. The rise time T_r of the pulse has an exponential relationship with the cable length L, while the step-up ΔU approximates a linear relationship with the cable length L.

This phenomenon may be attributed to the increase in both the capacitance and resistance of the entire cable as its length increases. The calculation of the cable's distributed parameters reveals that the time constant $\tau = RC$ of the cable system also increases. Consequently, the rate at which each layer of the cable responds to the pulse signal decreases, causing the shielding layer and sheath layer to require more time to recover from the pulse transient back to a steady state. This is specifically manifested as an elongation of the pulse rise time and an increase in the step-up during the pulse duration.

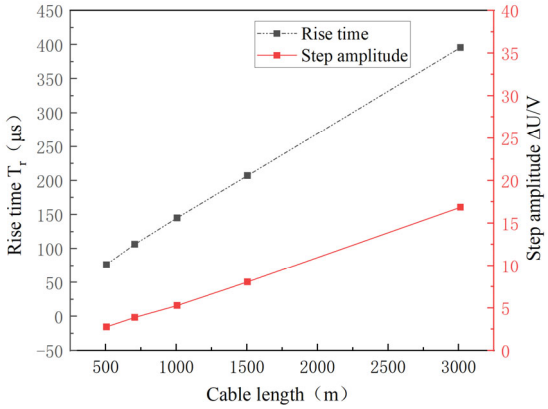


Figure 12. The characteristic parameters of the pulse signal vary with the length of the cable.

Using the Powergui module in MATLAB, the current waveforms of the fault section (0.05 s–0.07 s) were subjected to FFT analysis, resulting in the frequency spectrum shown Figure 13, along with the calculation of the THD. When insulation layer failure occurs in the cable, the direct current component and the contents of the second and third harmonics in the conductor layer and shielding layer currents increase. Additionally, the second, third, fourth, fifth, sixth, and seventh harmonic contents in the sheath layer current are significantly elevated.

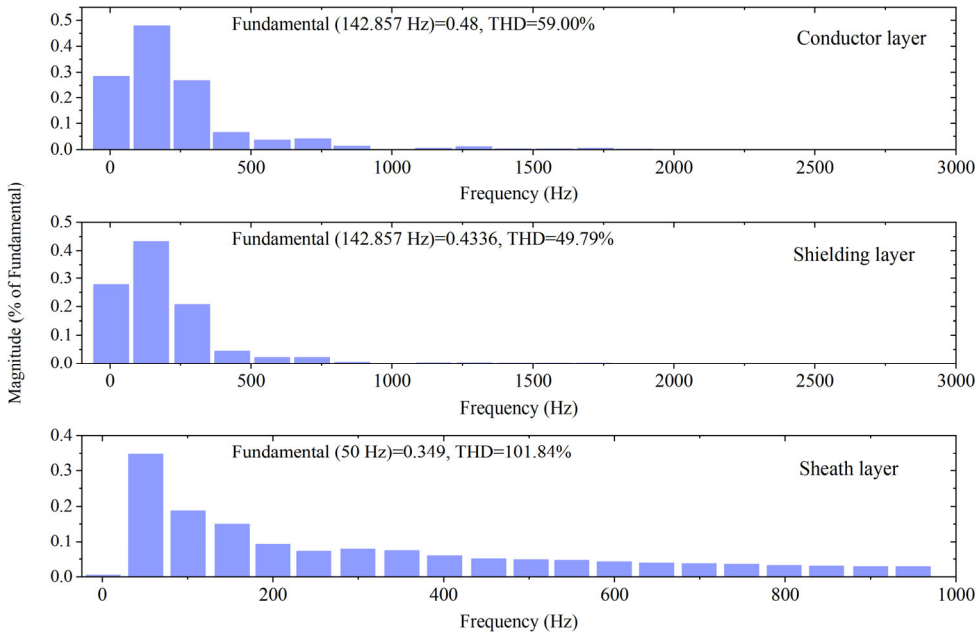


Figure 13. FFT analysis of current at each layer of fault loop.

5. Conclusions

This paper quantitatively analyzes the frequency variation patterns of the first and second parameters of a 10 kV cable during insulation layer aging and semiconductive layer aging and summarizes the impact of aging conditions on the input impedance spectrum of the cable. By utilizing a combined MATLAB-PSCAD simulation, the transient current characteristics of each layer under aged conditions are simulated, followed by harmonic distortion analysis. The main conclusions are as follows:

1. Among the secondary parameters of the cable, the attenuation coefficient is most significantly affected by insulation layer aging, increasing by 41.38% at a frequency of 1 MHz. The changes in characteristic impedance magnitude and wave speed are approximately between 20% and 22%.

2. For the cable's input impedance spectrum, insulation layer aging does not alter the periodicity of the spectrum but leads to the attenuation of characteristic peaks and a shift toward lower-frequency ranges.

3. Aging of the semiconductive layer results in a significant increase (over 10 times) in its relative permittivity at low frequencies, affecting the cable's characteristic impedance, attenuation coefficient, and wave speed only during the initial aging phase (0–22 days). In the later stages of aging (beyond 40 days), it has a negligible impact on the cable's carrier characteristics.

4. Aging failures of both the insulation layer and semiconductive layer induce induced pulse signals in the cable layers, which exhibit sensitivity to cable length, with significant increases in the second and third harmonic contents of the conductor and shielding layers.

Author Contributions: Conceptualization, M.W. and J.G.; methodology, X.Y. and Z.W.; software, J.L.; validation, X.Y. and Z.W.; formal analysis, X.Y.; investigation, Z.W.; resources, G.W.; data curation, Z.W.; writing—original draft preparation, M.W.; writing—review and editing, J.G.; visualization, X.G.; supervision, J.G.; project administration, X.Y. All authors have read and agreed to the published version of the manuscript.

Funding: This research received no external funding.

Data Availability Statement: The data presented in this study are available on request from the corresponding author.

Conflicts of Interest: Authors Xiaohua Yang, Jiahao Li and Guanpan Wang were employed by the company Yunnan Power Grid Co., Ltd. The remaining authors declare that the research was conducted in the absence of any commercial or financial relationships that could be construed as a potential conflict of interest.

References

1. Zhang, J.; Xue, P.; Xiang, B.; Gao, L.; Jiang, X. Influence of bubbles on electric field distribution of butt-gaps in superconducting cable insulation layer. *IET Gener. Transm. Distrib.* **2021**, *16*, 680–685. [CrossRef]
2. Swarnankur, G.; Supriyo, D. A generalized approach to deduce the impedance and admittance of underground cable containing N semiconductor screens. *Eng. Sci. Technol. Int. J.* **2022**, *28*, 101029.
3. Lv, Z.; Bian, L.; Feng, M.; Zhang, J. Capacity Analysis of Cable Insulation Crosslinking Production Process Based on IoT Big Data. *J. Phys. Conf. Ser.* **2022**, *2237*, 012028. [CrossRef]
4. Lu, H.; Zhu, F.; Liu, Q.; Li, X.; Tang, Y.; Qiu, R. Suppression of Cable Overvoltage in a High-Speed Electric Multiple Units System. *IEEE Trans. Electromagn. Compat.* **2019**, *61*, 361–371. [CrossRef]
5. Zhou, L.; Liu, C.; Quan, S.; Zhang, X.; Wang, D. Experimental study on ageing characteristics of electric locomotive ethylene propylene rubber cable under mechanical–thermal combined action. *High Volt.* **2022**, *7*, 792–801. [CrossRef]
6. Zieliński, D.; Grzechca, D. The Effect of Cable Aging on Surge Arresters Designed by Genetic Algorithm. *Appl. Sci.* **2023**, *13*, 11364. [CrossRef]
7. Reddy, A.S.; Kumari, S.M. A review of switching overvoltage modeling in UHV AC transmission lines. *Electr. Power Syst. Res.* **2024**, *236*, 110902. [CrossRef]
8. Fu, H.; Qiu, L.; Ai, Y.; Tu, J.; Yan, Y. Deep learning-based fault detection and loca-tion in underground power cables using resonance frequency analysis. In *Electrical Engineering*; Springer: Berlin/Heidelberg, Germany, 2024; pp. 1–12.
9. Jin, W.; Wang, D.; Gao, H.; Peng, F.; Guo, Y.; Gao, M.; Wang, J. Two-terminal traveling wave fault location approach based on frequency dependent electrical parameters of HVAC cable transmission lines. *Electr. Power Syst. Res.* **2024**, *235*, 110842. [CrossRef]
10. Barkhordari, S.M.; Fattahi, H.; Armaghani, J.D.; Muhammad Khan, N.; Afrazi, M.; Asteris, P.G. Failure mode identification in reinforced concrete flat slabs using advanced ensemble neural networks. In *Multiscale and Multidisciplinary Modeling, Experi-ments and Design*; Springer: Berlin/Heidelberg, Germany, 2024; pp. 1–15.
11. Mehti, C.; Elmir, B.; Khikmat, A. Investigation of Dielectric Properties and Structural Changes in XLPE Composite Insulation of Covered Conductor due to Thermal Aging. *Mater. Sci. Forum* **2024**, *1119*, 13–24.
12. Rashid, Z. Calculation of overhead and underground cable parameters at harmonic frequencies. *Electr. Eng.* **2020**, *103*, 729–741. [CrossRef]
13. Zhu, K.; Lee, W.K.; Pong, P.W. Energization-Status Identification of Three-Phase Three-Core Shielded Distribution Power Cables Based on Non-Destructive Magnetic Field Sensing. *IEEE Sens. J.* **2017**, *17*, 7405–7417. [CrossRef]
14. Le, J.; Wang, C.; Zhou, W.; Liu, Y.Y.; Cai, W. A novel PLC channel modeling method and channel characteristic analysis of a smart distribution grid. *Prot. Control. Mod. Power Syst.* **2017**, *2*, 14. [CrossRef]

15. Corchado, A.J.; Cortés, A.J.; Cañete, J.F.; Díez, L. An MTL-Based Channel Model for Indoor Broadband MIMO Power Line Communications. *IEEE J. Sel. Areas Commun.* **2016**, *34*, 2045–2055. [CrossRef]
16. Ji, M.; Colin, X.; Liu, W.; Chi, X.; Chatenet, S.; Wei, W. Comparison of the performances and aging mechanisms of XLPE and EVA insulation during their thermal oxidative aging. *Polym. Degrad. Stab.* **2024**, *222*, 110699. [CrossRef]
17. Shimomura, K.; Sato, M. General Criterion for Non-Hermitian Skin Effects and Application: Fock Space Skin Effects in Many-Body Systems. *Phys. Rev. Lett.* **2024**, *133*, 136502. [CrossRef] [PubMed]
18. Su, J.; Wei, L.; Zhang, P.; Li, Y.; Liu, Y. Multi-type defect detection and location based on non-destructive impedance spectrum measurement for under-ground power cables. *High Volt.* **2023**, *8*, 977–985. [CrossRef]
19. Liu, T.; Liu, T.; Li, X.; Wei, Y.; Zhu, Y.; He, J.; Li, G. Effect and mechanism analysis of matrix resin type on thermal aging characteristics of semi-conductive shielding material for high voltage cable. *J. Appl. Polym. Sci.* **2024**, *141*, e55311. [CrossRef]
20. Li, J.; Gao, Y.; Song, Z.; Liu, B.; Guo, C.; Chen, Y.; Du, B. Study on thermal cycling ageing resistance of performances of polypropylene/elastomer/boron nitride nanocomposites for high voltage direct current cable insulation. *High Volt.* **2024**, *9*, 556–565. [CrossRef]

Disclaimer/Publisher's Note: The statements, opinions and data contained in all publications are solely those of the individual author(s) and contributor(s) and not of MDPI and/or the editor(s). MDPI and/or the editor(s) disclaim responsibility for any injury to people or property resulting from any ideas, methods, instructions or products referred to in the content.